Self-formed Quantum Wires and Dots in GaAsP-GaAsP Core-Shell Nanowires
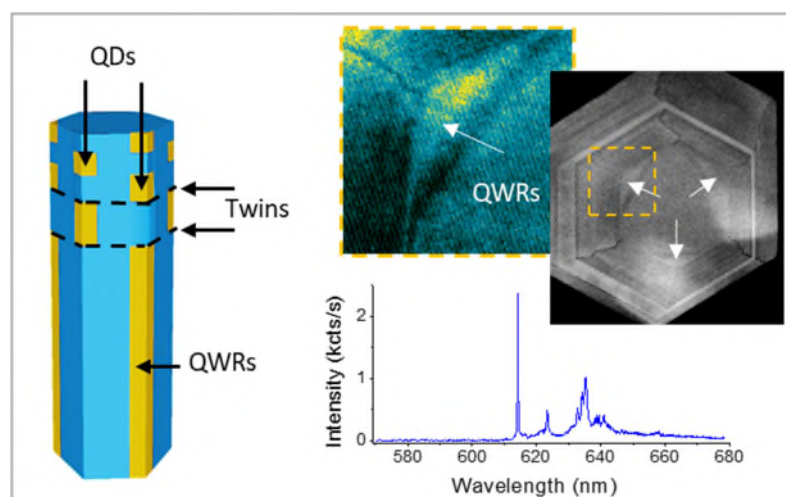
H. Aruni Fonseka[1]*, Anton V. Velichko[2], Yunyan Zhang[3], James A. Gott[1], George D. Davis[2], Richard Beanland[1], Huiyun Liu[3], David J. Mowbray[2] and Ana M. Sanchez[1]*

[1]Department of Physics, University of Warwick, Coventry CV4 7AL, United Kingdom

[2] Department of Physics and Astronomy, University of Sheffield, Sheffield, S3 7RH, United Kingdom

[3] Department of Electronic and Electrical Engineering, University College London, London WC1E 7JE, United Kingdom

ABSTRACT: Quantum structures designed using nanowires as a basis are excellent candidates to achieve novel design architectures. Here, triplets of quantum wires (QWRs) that form at the core-shell interface of GaAsP-GaAsP nanowires are reported. Their formation, on only three of the six vertices of the hexagonal nanowire, is governed by the three-fold symmetry of the cubic crystal on the (111) plane. In twinned nanowires the QWRs are segmented, to alternating vertices, forming quantum dots (QDs). Simulations confirm the possibility of QWR and QD-like behaviour from the respective regions. Optical measurements confirm the presence of two different types of quantum emitters in the twinned individual nanowires. The possibility to control the relative formation of QWRs or QDs, and resulting emission wavelengths of the QDs, by controlling the twinning of the nanowire core, opens up new possibilities for designing nanowire devices.

Over the past two decades, semiconductor nanowire architectures have been investigated as an alternative to thin films due to advantages which include, a larger active surface area with smaller foot print, lower material consumption, intrinsic formation of an optical cavity and the ability to tolerate higher levels of strain without dislocation formation[1-3]. Semiconductor nanowires allow the formation of heterostructures in all three directions, namely, along the growth axis and side facets, making them versatile building blocks in the design of complex device structures[4]. The possibility of growth on multiple facets may result in the formation of unintentional features. Those that form on the side facets and vertices of nanowires by vapour-solid (VS) growth can be considered analogous to growth on non-planar surfaces in thin film structures, where formation is driven by growth rate anisotropy on different facets, strain, differences in surface diffusion of adatoms, capillary effects arising from shape and entropy of mixing in alloys[5-7]. Composition inhomogeneities may also occur for alloy nanowires in the axial direction, due to different diffusion lengths of the different atomic species[8], and, for nanowires grown by the vapour-liquid-solid (VLS) mechanism, unintentional core-shell structures may form due to different incorporation rates of species during the VLS and simultaneous VS growth mechanisms[9, 10]. Some of these unintentional features have been shown to

exhibit optical properties consistent with quantum structures, many of which with superior quality to those intentionally grown structures [11-17].

Quantum wires (QWRs) formed along the vertical edges of the nanowires have been demonstrated in the GaN-AlN material system.[12, 13] Here, it has been shown that the efficient charge transfer from the relatively large nanowire core enables high intensity luminescence from the QWRs, despite their small material volume[13]. This demonstrates an advantage of the QWRs integrated to a nanowire template. Another advantage of such QWRs formed on nanowire templates is the ease of formation and control, compared to techniques such as template assisted growth, top-down etching and VLS growth, commonly used to form QWRs[18-21].

Quantum dots (QDs) are another structure that is reported to be self-assembled on nanowires[11, 14-17]. Here too, being hosted by a nanowire has proven to be advantageous in terms of subsequent photon extraction, as the host nanowire can be designed as an efficient photon out-coupler[22]. The 3-dimensional nature of the host nanowire is also beneficial in sensor applications as QDs can be placed in multiple directions, increasing sensor area as well as reducing the directionality compared to planar QD sensors[23]. Therefore, embedding of quantum structures within nanowires has many advantages, and their self-assembly have proven to bring unexpected benefits in terms of their structural and optical properties.

This work presents novel types of self-formed GaAsP QWRs and QDs in [111] grown GaAsP-GaAsP core-shell nanowires. The two types of structures are related and can be simply controlled by twinning of the host nanowire. The QWRs are formed as triangular cross-sectional GaAsP filaments that are demarcated by P rich bands and run along the edges of the GaAsP host nanowire (which will be referred to as the 'nanowire' henceforth) core. In contrast to previously reported QWRs formed on nanowires[12, 13], these QWRs only form on three of the six vertical nanowire edges. This enables the isolation and segmentation of the QWRs by twin planes in the nanowire, leading to the formation of QDs. Single band effective mass simulations and photoluminescence measurements confirm their respective QWR and QD-like behaviours.

RESULTS AND DISCUSSION:

Figure 1 (a) shows a scanning electron microscope (SEM) image of the core-multi-shell nanowires, and a schematic of the nominal structure with GaAsP core, inner GaAsP shell, GaAs quantum well (QW) and outer GaAsP shell. The nanowires are around 5.5 µm in length and their tips are slightly thicker than the bases. Figure 1 (b) shows a typical 6 K micro photoluminescence (µ-PL) spectrum from the middle of a single nanowire. Bright emission is observed in the 720 – 780 nm range from the GaAs QW. Further details on this structural component will be discussed elsewhere[24]. In addition to the GaAs QW emission, a number of comparatively sharp, less intense, higher energy lines are observed in the 610 – 650 nm wavelength range. These lines are consistent with emission by a small number of quantum emitters.
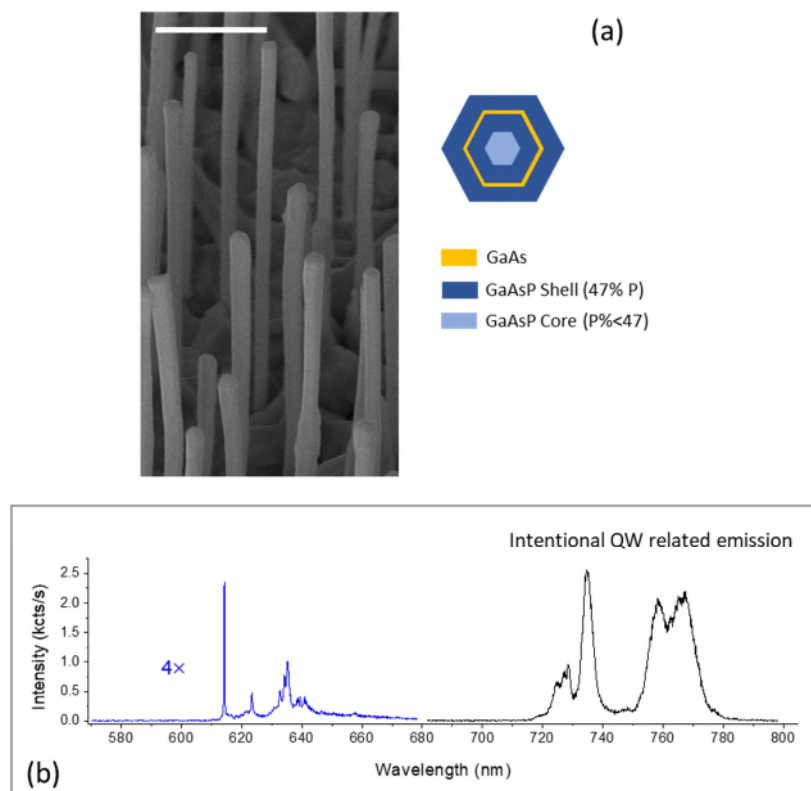

Figure 1. (a) SEM image of the nanowires with the inset showing a schematic of the intended cross-section. Scale bar is 1 µm. (b) A single nanowire PL spectrum obtained at 6 K. Sharp, less intense peaks are observed in the 610 – 650 nm wavelength region and the intentional QW emission is visible in the 720 – 780 nm range.

A detailed structural analysis of the nanowires was performed to determine their nanoscale structure and to identify the origin of the short wavelength emission. Figure 2 (a) shows a low magnification bright field (BF) transmission electron microscopy (TEM) image of a typical nanowire, with insets showing higher magnification images from the bottom, middle and upper regions of the nanowire. The bottom third of the nanowire is defect-free, with zinc-blende (ZB) crystal structure. Twin boundaries start to appear in the middle third, with the twinning frequency increasing towards the top of the nanowire. The uppermost third of the nanowire is heavily defective, as shown in the inset of Figure 2(a).

Due to the sequential nature of the microtome slicing, the position of each section along the nanowire can be identified, relative to its base (see Section S1 in supplementary information (SI)). Figure 2 (b), shows an annular dark field (ADF) scanning transmission electron microscopy (STEM) image of a nanowire cross section taken from the defect free bottom third of a nanowire. Contrast in this image is related to atomic number, with materials with higher atomic number in brighter contrast. Hence, GaAsP materials with higher P (lower As) content appear darker in Figure 2 (b). The intentional GaAs QW can be seen in bright contrast, between the two GaAsP shells and the inset Fourier transform shows that the nanowire facets are of {110} type. Alloy fluctuations, that are occasionally observed in molecular beam epitaxy grown AlGaAs[25] and GaAsP[26] nanowire shells, are also observed in the VS grown GaAsP shells, as striations marked in Figure 2 (b).

In addition, triangular regions demarcated by darker bands can be seen at three alternating vertices closer to the GaAsP core of the nanowire (see Figure 2 (b)). Around two thirds of the nanowire cross-sections examined showed these features. As the facets of the nanowire are of {110} type, the radial directions joining the vertices of the hexagonal cross section are of the partially polar <112> type, alternating between A and B polarities. The polarity of the radial directions which pass through the vertices of the triangles have been identified and verified, as described under section S2 in the SI, and this result is consistent with the polarity of the directions of the alternating dark and light P rich radial lines that have been reported in GaAsP shells previously[26] (which is in opposite to other common III-III-V type nanowires shells [27, 28]). The observed triangular regions are formed along

<112>B directions, with the P rich bases of the triangular regions forming on the {112} B facets, as shown in the schematic in Figure 2 (c).

Consecutive microtome sections from the same nanowire were studied in order to ascertain the three-dimensional form of these triangular features. Figures S3 (c) and (d) show two microtome slices from the bottom third of the nanowires, that are separated by approximately 150 nm. The same nanowire can be identified by its relative position with respect to neighbouring nanowires, as shown by the respective coloured circles. As Figures S3 (g) and (h) illustrate, a triangular feature of a similar size is present in both sections of the selected nanowire, establishing its 'wire' like form along the edges of the GaAsP nanowire core.
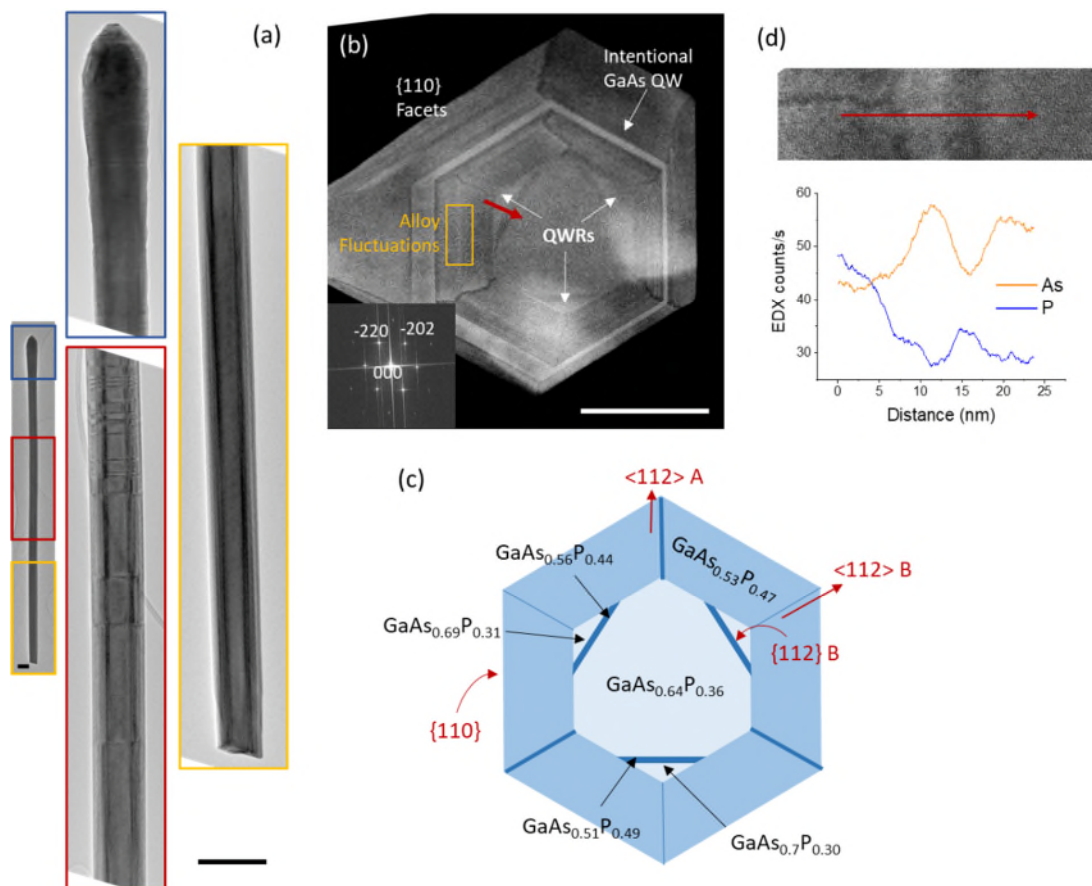

Figure 2. (a) BF TEM images from the base (yellow), middle (red) and tip (blue) sections of a nanowire. The base is defect-free, the middle is twinned with increasing twin density towards the top, while the tip is heavily defective. Scale bars are 200 nm. (b) A cross-section ADF STEM image from the bottom third of a nanowire showing triangular regions demarcated by P-rich bands at three of the alternating vertices. Inset shows the Fourier transform of the main image confirming {110} type side facets. Scale bar is 50 nm. (c) Schematic of the cross section in (b), indicating the

polarities of the facets and compositions determined by EDX from a representative nanowire. (d) EDX line scan along the red arrow indicated in (b).

Figure 2 (d) shows the composition measured by energy dispersive X-ray (EDX) along a line crossing the triangular region, indicated by the red arrow in Figure 2 (b). This confirms that the dark band corresponds to a P rich region while the triangular region is a relatively As rich area bound by the P rich band and relatively P rich GaAsP shell. The schematic in Figure 2 (c) gives compositions measured in a single typical nanowire. Similar measurements on multiple nanowires showed that the core and QWR compositions vary considerably, while the GaAs$_{1-x}$P$_x$ shell composition remained constant at $x \approx 0.47$. The core has an As composition 4 - 12 % higher compared to the shell, while the As composition of the triangular regions can be 2-17 % higher than that of the shell. As a result, the As composition of the triangular regions can be higher or lower than that of the core, with variation within the triangular regions of the same nanowire. However, the As composition of the triangular regions always remains higher than that of the shell. This considerable variation in composition between nanowires could be one reason for these triangular regions to be unobserved in some nanowires, when the composition differences fall below the sensitivity of the EDX measurements.

Since P-rich material has a higher bandgap, the dark bands visible in Figure 2 (b) can act as barriers to carrier transport. Thus, the relatively As-rich triangular wires demarcated by the {112} B P-rich bands could act as quantum wires (QWRs) and produce luminescence in the 610 -650 nm range, that is seen in Figure 1 (b). In order to verify this hypothesis, their electronic structure was simulated using the single band effective mass approximation. Figure 3 (a) shows the schematic of the approximated structure of the triangular region used for the simulations. The outer GaAs$_{0.53}$P$_{0.47}$ shell is considered to be sufficiently thick that it remains unstrained. The remainder of the structure is considered to be strained with respect to the shell. As discussed above, and similar to previous report on self-formed GaN QWRs[12], the current wires exhibit a significant variation in size (between different nanowires and within the same nanowire). In addition to this, in the current case, the associated compositions also vary as discussed previously. Hence, the variations observed in dimension and composition across the nanowire population were modelled with four parameters,

compositions - C_2, C_3, C_4 and triangle height D_4. These parameters and their respective ranges considered are shown in Figure 3 (a).
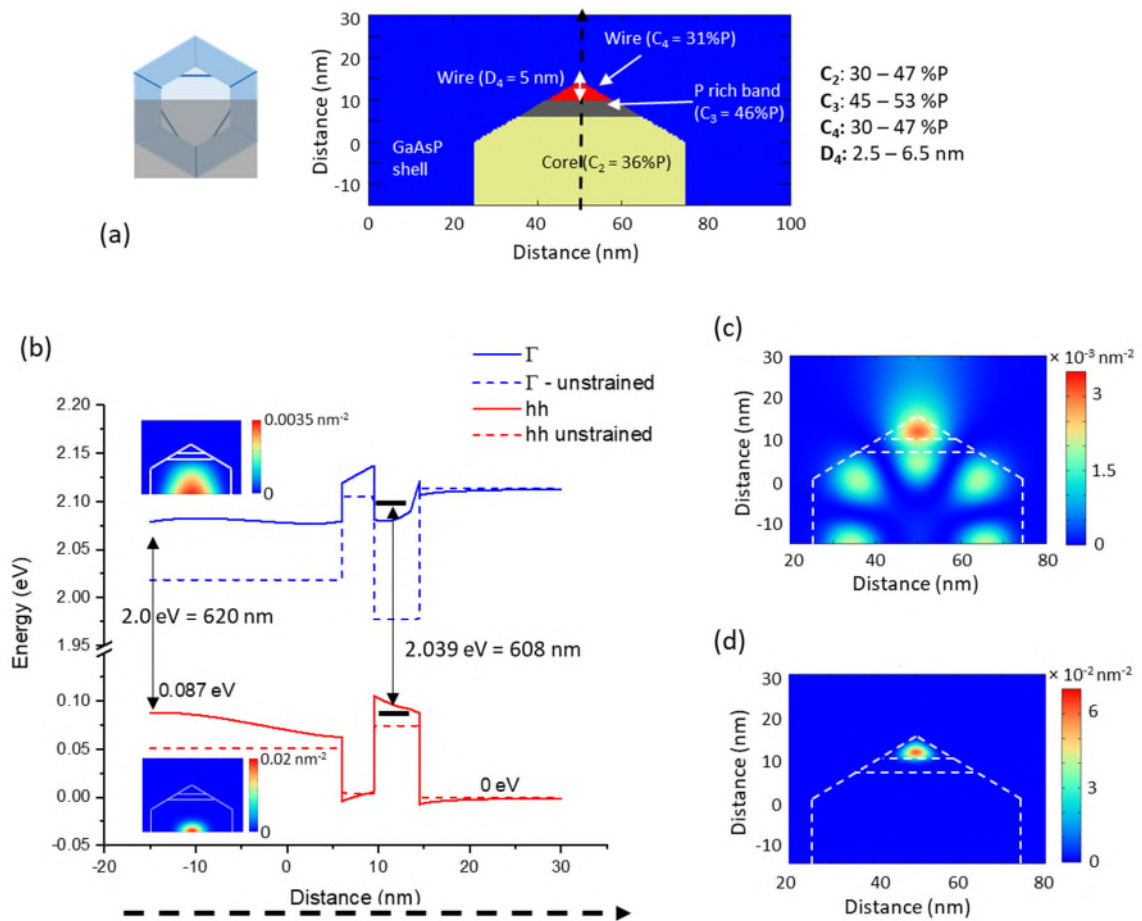

Figure 3. (a) The schematic of the approximated structure of a part of the nanowire that includes a single triangular region. The ranges of the parameter values considered are also shown. (b) Solid lines – variation of conduction and valence band edges along the black dashed line shown in (a), dashed line – conduction and valence band edges along the same line, but without including the effect of strain. The simulations are carried out for a lattice temperature of 6 K. Probability densities in the insets show the lowest electron and highest hole states localised in the nanowire core. (c) and (d) Probability densities for the lowest electron and highest hole states confined to an As rich triangular region with compositions equal to the average of the two shown in Figure 2 (c), respectively. White dashed lines indicate the position of the triangular wire region.

Since the GaAs-GaP material system has a high lattice mismatch, the effect of strain is significant. Figure 3 (b) shows the conduction and valence band edges (solid lines) along a line passing through the vertex of the triangular region (black dashed line in Figure 3 (a)), with parameter values equal to the averages of the two shown in Figure 2 (c). The dashed lines show the same band edges, but without including strain. It is clear that the effects of strain arising from the relatively large

8

GaAsP shell is significant. The two dimensional strain distribution is found to be complex. The strain maps ε_{xx} and ε_{yy} for the same compositions as above, and a comparison of the simulation with an experimentally obtained strain map are given in SI Figure S4.

The overall form of the electronic structure of these triangular cross-sectioned filaments is found to result from the complex interplay between composition, strain and quantum confinement. Although the As composition of the triangular region is always greater than that of the shell it can be either less or greater than that of the core. When strain and confinement is taken into account, the band gap of the triangular region may either be larger or smaller than that of the GaAsP core. Although the conduction band edge may be above and valence band edge may be below that of the core, localised electron states can be formed within the triangular regions, enabling them to act as electronic QWRs. Such different band alignment and confinement scenarios, arising from different parameters sets of composition and size are discussed in Section S5 in the SI. For most scenarios considered, the triangular regions are able to confine both electrons and holes and therefore should result in optically active QWRs, subject to these being able to capture photoexcited carriers.

For the structure discussed in Figures 2 (c) and 3 (b), the lowest energy electron and hole states lie in the nanowire core, while higher energy states are localised within the triangular QWR region. The probability densities of the lowest energy electron and highest energy hole states localised in the QWR region are shown in Figures 3 (c) and (d), respectively. The emission wavelength, calculated for the average QWR taken from Figures 2 (c) and 3 (b), is 608 nm ($\equiv 2.039$ eV), and for the nanowire core 620 nm ($\equiv 2.001$ eV) - blue shifted with respect to the unstrained value of 629 nm ($\equiv 1.972$ eV). For the range of parameters considered, the QWR emission wavelength is calculated to vary between 595 and 613 nm, and that of the core between 620 – 640 nm.
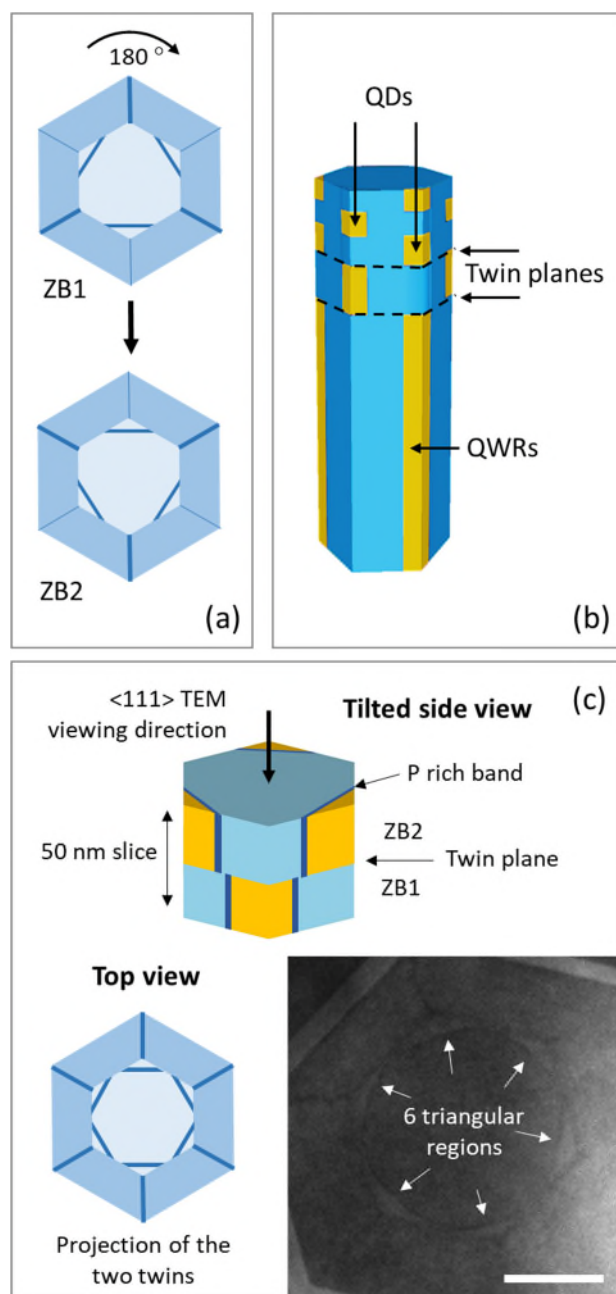
Figure 4. (a) Schematics of the transpose of QWRs to alternate vertices with twin rotation. (b) Segmentation of QWRs and formation of QDs with sequential twinning of the nanowire. (c) Schematic of a microtome slice containing a twin. Insets show the expected projection in the axial view and an ADF STEM image from the middle of a nanowire showing six triangular regions, instead of three. Scale bar is 20 nm. The GaAsP shell is not shown in the 3D schematics in (b) and (c) for clarity.

Having confirmed that the observed triangular structures can form optically active QWRs, the effect of twinning on their structural and optical properties are now considered. A twin perpendicular to the growth direction in a [111] nanowire can be considered as a 180 ° rotation of the crystal about its growth axis. As shown by the schematic in Figure 4a, this transposes the three QWRs to alternate

vertices, swapping the <112>A and <112>B radial directions. Consecutive twins truncate the QWRs along the axial direction, as shown in Figure 4 (b), and when a twin segment is sufficiently small, confinement along the axial direction may result in the formation of QDs. The formation of QDs with different heights, resulting from increasing twinning frequency, as in the current sample is depicted in Figure 4 (b). It should be noted that two additional requirements need to be fulfilled for the QWR segments to form optically active QDs. First, the As-composition of the QWRs should be higher than that of the core to produce confinement along the axial [111] direction. Second, the triangular QWR cross-sections should be sufficiently small not to overlap with those at the alternative vertex of the adjacent twin, as this would result in coupling between QDs across twin boundaries. Figure 4 (c) shows an axial section from the twinned middle third of the nanowire (2.5 to 3 µm from the base). Six triangular regions instead of three are clearly visible due to the projection of QWR segments in both twins within the ~50 nm thick slice. In this case, there is no overlap between them, consistent with one of the requirements for the formation of QDs. This is schematically depicted in Figure 4 (c).

In order to estimate the expected emission from these QDs, simulations were carried out on a structure created by isolating a QWR segment similar to that in Figure 3 (a), within a GaAsP core in the [111] direction (Figure S5 (a) in SI). The emission wavelength extracted for a dot with 8 nm height and lateral dimensions and compositions similar to the QWR in Figure 3 (a) is 582 nm ($\equiv$ 2.129 eV), 26 nm blue shifted with respect to that of the respective QWR due to the additional confinement in the axial direction. Respective probability densities for electrons and holes are shown in Figure S5 (b) and (c).

The above results provide an explanation for the high energy emissions observed from these nanowires and predict that this emission could have QWR and QD characteristics. Detailed µ-PL measurements were carried out in order to further confirm the link between the 610 – 650 nm emissions and the nanoscale structure of these nanowires. PL spectra were collected from nine different nanowires at a sample temperature of 6K and with an incident laser spot size ~1-2 µm, allowing the spatial variation of the emission to be studied as the excitation was moved along the nanowire. Around half the nanowires studied exhibit emission only when excited within the first 1-2

µm from the base. As structural studies indicate the formation of QDs by twinning in the central third of some of the nanowires, here, we concentrate on nanowires that exhibit emission when excited in this region.
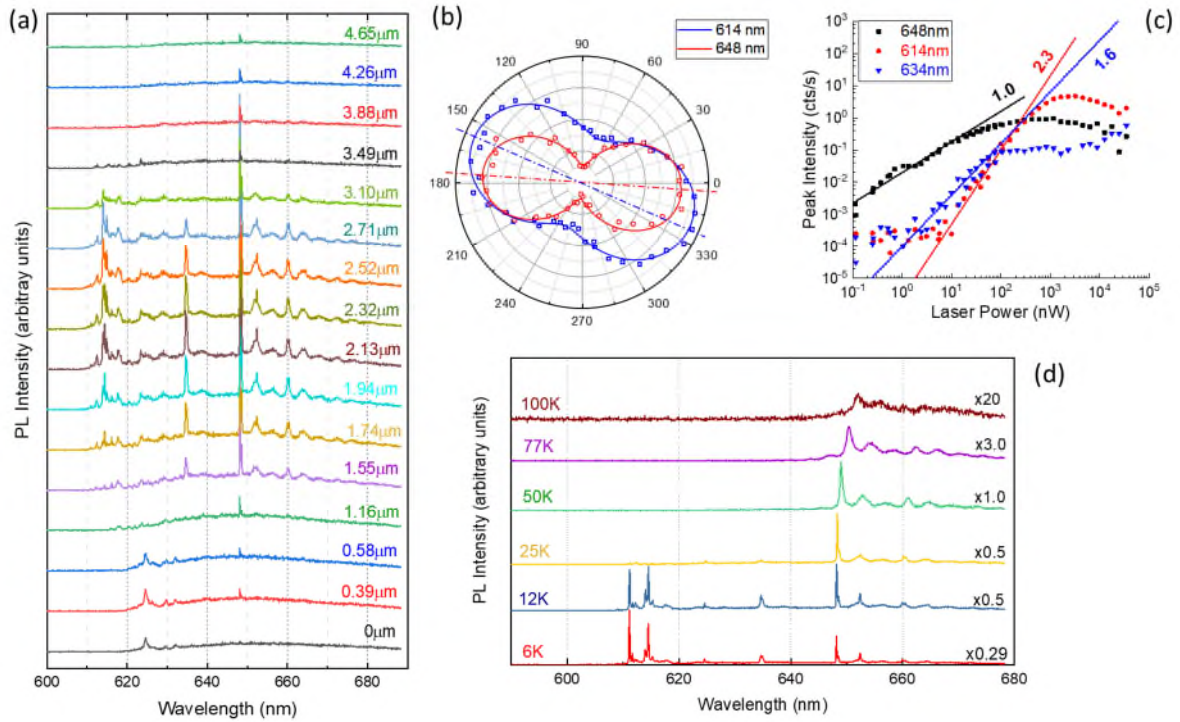

Figure 5. (a) µ-PL spectra recorded for different positions along the axis of a nanowire for a laser power of 50 nW. Distances are given with respect to the base. (b) Polarisation plots for two of the sharp emission lines from (a). The axis of the nanowire is horizontal, and the axis of the preferred polarisation is indicated by the dashed lines in respective colours. (c) Log scale plot of the power dependent intensity of three of the sharp emission lines. (d) µ-PL spectra as a function of the sample temperature. The numbers on the right hand side give the multiplication factor for each spectrum.

Figure 5 (a) shows µ-PL spectra excited for different spatial positions along the length of an aforementioned nanowire (different to that shown in Figure 1 (b)). The emission consists of a small number of sharp lines, the relative intensities of which vary with excitation position. Line widths as low as ~80 µeV, which are close to the spectral resolution of the measurement system were measured. As the number of emission lines is relatively small, they are not consistent with the alloy fluctuations observed in the shell (Figure 2(b))[25, 29]. Furthermore, as those alloy fluctuations are present along the entire length of the nanowire, they should not show a strong spatial variation as seen here. For the current nanowire, the strongest emission is at 648 nm. This line is observed at all points along the

nanowire, although its intensity becomes weaker at either end. The lines to longer wavelength follow the same spatial intensity behaviour as the 648 nm line. The similar behaviour of this set of lines suggests a common origin.

Lines to shorter wavelengths exhibit a more complex behaviour, with the majority only observed for excitation towards the centre of the nanowire and with a stronger variation in relative intensity as the excitation position is altered. In addition to the sharp emission lines there is a weak but broad underlying background emission which extends between approximately 620 and 680 nm. The most likely origin of this emission is the central GaAsP core.

In order to probe further the origin of the sharp 610-670 nm emission lines, polarisation and power-dependent measurements were performed with the laser spot focused on the middle of the nanowire. Figure 5 (b) shows polarisation dependent behaviour of a lower wavelength and a higher wavelength peak. The emission at 648 nm (and lines to longer wavelengths) are preferentially polarised along the nanowire axis. In contrast, lines at shorter wavelengths are not as strongly polarised and their polarisation axes are inclined to that of the nanowire by up to 30 °. Figure 5 (c) shows the continuous wave laser excitation power dependence of three emission lines. All lines exhibit an initial increase in intensity with increasing power, with saturation at high powers and, in some cases, a decrease. The majority of lines exhibit an initial linear behaviour consistent with single exciton recombination (either charged or uncharged), but a number of shorter wavelength lines show quadratic or cubic behaviour, consistent with higher order excitonic processes[30]. Figure 5 (d) shows μ-PL spectra as a function of temperature between 6 and 100K. The emission lines below 640 nm are very temperature sensitive and their intensity is almost fully quenched by 25K. In contrast, the longer wavelength lines (> 640 nm) persist to significantly higher temperatures, displaying broadening and a bandgap related red shift for temperatures above 50K.

The optical spectra of Figure 5 (a) and (d) suggest two different types of quantum emitters. The longer wavelength lines, which show a similar spatial variation, are polarised parallel to the nanowire axis. This is consistent with QWRs running along the length of the nanowires, as this polarisation behaviour is expected due to shape anisotropy. The multiple lines may result from

different charged exciton species and/or the three QWRs on the different facets. The shorter wavelength lines are only observed for excitation of the middle of the nanowire, the region expected to contain the twin induced QDs. Their polarisation is expected to be only partly dependent on their height-to-width ratio, and will not necessarily lie along the nanowire axis, as is observed experimentally. The blue-shift of the higher energy QD-like lines with respect to that of the QWR-like emission is consistent with the 20 – 30 nm blue shift predicted by the calculations for QD structures formed by multiple twinning. The overall blue shift observed between calculated and experimental absolute values obtained for the QWRs, QDs and core is most likely due to the assumed idealised structure used for the simulations. For example, the strain is more likely to be distributed between the core and the shell, decreasing bandgaps of both, core and shell, and hence red shifting the experimentally observed emissions.

Although the optical data is largely consistent with the two different types of quantum emitters, Figure 5 (a) shows that the QWR emission is weaker at either end of the nanowire in comparison to the centre. This is in apparent disagreement with the structural studies which show QWR formation at one end (base) of the nanowire. This may be caused by enhanced non-radiative recombination at the broken bottom end of the nanowire which would degrade the QWR emission intensity. Another discrepancy is the QD-like power dependence of the longer wavelength lines, that are otherwise attributed to QWR-like emissions. This suggests the existence of compositional and dimensional fluctuations along the QWRs that result in them being broken into elongated segments that act as QDs. With the current knowledge of structure (discussed in relation to Figure 2) it seems reasonable to assume that such fluctuations are possible.

The formation of previously reported triangular QWRs within nanowires has been attributed to preferential nucleation of the QWR material on selected facets of the preceding structure[12]. QWR formation is observed on all six edges in these wurtzite (WZ), GaN-AlN nanowire templates due to all six *a* plane facets in the WZ crystal structure, where QWRs have nucleated being identical. Also, in the case of reference 12, effects from segregation of alloys is absent due to both materials involved being binary. The present observation of QWR formation on only three alternating edges, and the

14

resulting unique ability to form QDs by twinning, arises from the two different partial polarities of the {112} facets in the ZB crystal structure, and the possibility of the two polarities to have different properties, such as different growth rates, decomposition rates and diffusion lengths[31-33]. A detailed growth mechanism for the formation of these features is proposed in Section S7 in the SI.

CONCLUSIONS:

In summary, a novel form of self-assembled QWRs that form on the three {112} B faceted edges of GaAsP nanowires is presented. The QWRs converts to QDs via sequential twinning of the nanowire core owing to being restrained to only three of the six edges. Band structure simulations confirm the possibility of both types of structures being optically active emitters, and polarisation, power and temperature dependent PL measurements are consistent with the respective QWR and QD-like optical behaviours. The QD emission can potentially be tuned using controlled twinning that has been demonstrated in previous works[34]. Overall, these nanowires demonstrate an architectural system where optically active QWs, QWRs and QDs can be formed within the same nanowire.

EXPERIMENTAL METHODS:

The GaAsP-GaAsP core-shell nanowire sample was grown by solid-source molecular beam epitaxy (MBE) on Si (111) substrates. The GaAsP nanowire core was self-catalysed using Ga droplets and the Ga beam equivalent pressure was 8.41×10^{-8} Torr, while the V/III and P/(P+As) flux ratios were maintained at 40 and 25%, respectively. The nanowire core was grown at 640 °C for 90 mins. Ga particle solidification was carried out for one hour in three steps following the core growth at the same temperature, but with the Ga beam switched off. As and P fluxes were reduced to 0.68×10^{-6} and 0.35×10^{-6} Torr for the first 30 min and increased to 2.21×10^{-6} and 2.32×10^{-6}, 5.11×10^{-6} and 5×10^{-6} Torr, respectively for the following two 15 min steps. The Ga beam equivalent pressure, V/III flux ratio and P/(P+As) for the shell growth were 8.41×10^{-8} Torr, 50 and 50%, respectively. The shell growth was carried out for one hour at 550 ° C. Following the first shell, an intentional GaAs QW and a second GaAsP shell was grown. Details of these growth steps will be published elsewhere[24]. Growth

details of these layers will not be discussed in the current work as the feature of interest is formed within the first shell and is not influenced by the subsequent layers as discussed under the results section.

The morphology of the nanowires was analysed using a Zeiss Gemini 500 Scanning Electron Microscope operating at 5 kV. Detailed structural and compositional analysis was carried out in transmission and scanning modes with Jeol 2100 and doubly corrected Jeol ARM200F transmission electron microscopes, both operating at 200 kV. Compositional analysis was carried out using a 100 mm^2 Oxford Instruments windowless EDX detector installed within the Jeol ARM200F microscope. Nanowire cross sections were prepared by embedding them in low viscosity resin followed by microtome slicing along its length. The slices were approximately 50 nm thick.

Simulations of the electronic structure of the QWRs and QDs were performed using nextnano© simulation software for semiconductor nanodevices [35]. Specific details of parameters used is given under the relevant section in Results and Discussion.

Micro-photoluminescence (µPL) measurements were carried out at 6 K, by focusing the incident laser to a spot size of 1-2 µm diameter using a 20x long working distance microscope objective. Nanowires were removed from the original substrate and transferred to a horizontal orientation on a new Si substrate. µPL spectra of single nanowires were excited by a continuous wave 515 nm solid-state diode laser. The samples were measured under vacuum inside a continuous flow cryostat with base temperature of 6 K. The PL was collected by the same microscope objective and focused into a 0.75 m spectrometer, where the spectral components were resolved and detected using a 300 lines/mm grating and a nitrogen cooled CCD. The spectral resolution was ~0.5 meV. Higher resolution measurements were recorded using an 1800 lines/mm grating with a resolution of 0.09 meV.

ASSOCIATED CONTENT

Supporting Information. Lateral cross-sectional TEM sample preparation process using microtome sectioning, polarity determination of the cross-sections, determination of the 3-dimensional form of the triangular regions using consecutive microtome sections, simulated 2-dimensional strain maps of the QWR structures, types of optical behaviour expected from the axial wires formed at the edges of the GaAsP nanowire cores, single band effective mass simulations of the QD structures formed by the consecutive twinning of the nanowire, proposed growth mechanism of the QWRs. This material is available free of charge via the Internet at http://pubs.acs.org.

AUTHOR INFORMATION

Corresponding Authors

*a.fonseka.1@warwick.ac.uk, *a.m.sanchez@warwick.ac.uk

Author Contributions

HAF, JAG, RB and AMS carried out the structural characterisations of the nanowires. YZ and HL grew the samples. HAF performed the optical simulations. AVV, GDD and DJM carried out the optical analysis. AMS, DJM and HL supervised the project. HAF and DJM prepared the manuscript with input from all authors.

REFERENCES

1.   Yan, R.; Gargas, D.; Yang, P. Nanowire photonics. *Nature Photonics* 2009, 3, 569-576.

2.   Eaton, S. W.; Fu, A.; Wong, A. B.; Ning, C.-Z.; Yang, P. Semiconductor nanowire lasers. *Nature Reviews Materials* 2016, 1, 16028.

3.   Otnes, G.; Borgström, M. T. Towards high efficiency nanowire solar cells. *Nano Today* 2017, 12, 31-45.

4.   Hyun, J. K.; Zhang, S.; Lauhon, L. J. Nanowire Heterostructures. 2013, 43, 451-479.

5.   Biasiol, G.; Gustafsson, A.; Leifer, K.; Kapon, E. Mechanisms of self-ordering in nonplanar epitaxy of semiconductor nanostructures. *Physical Review B* 2002, 65, 205306.

6.   Zhang, Q.; Voorhees, P. W.; Davis, S. H. Mechanisms of surface alloy segregation on faceted core-shell nanowire growth. *Journal of the Mechanics and Physics of Solids* 2017, 100, 21-44.

7.   Sköld, N.; Wagner, J. B.; Karlsson, G.; Hernán, T.; Seifert, W.; Pistol, M.-E.; Samuelson, L. Phase Segregation in AlInP Shells on GaAs Nanowires. *Nano Letters* 2006, 6, 2743-2747.

8.   Zhou, C.; Zheng, K.; Chen, P.-P.; Lu, W.; Zou, J. Unexpected formation of a hierarchical structure in ternary InGaAs nanowires via "one-pot" growth. *Nanoscale* 2017, 9, 16960-16967.

9.   Chen; Shehata, S.; Fradin, C.; LaPierre, R.; Couteau, C.; Weihs, G. Self-Directed Growth of AlGaAs Core−Shell Nanowires for Visible Light Applications. *Nano Letters* 2007, 7, 2584-2589.

10.   Guo, Y.-N.; Xu, H.-Y.; Auchterlonie, G. J.; Burgess, T.; Joyce, H. J.; Gao, Q.; Tan, H. H.; Jagadish, C.; Shu, H.-B.; Chen, X.-S.; Lu, W.; Kim, Y.; Zou, J. Phase Separation Induced by Au Catalysts in Ternary InGaAs Nanowires. *Nano Letters* 2013, 13, 643-650.

11.   Yu, Y.; Dou, X.-M.; Wei, B.; Zha, G.-W.; Shang, X.-J.; Wang, L.; Su, D.; Xu, J.-X.; Wang, H.-Y.; Ni, H.-Q.; Sun, B.-Q.; Ji, Y.; Han, X.-D.; Niu, Z.-C. Self-Assembled Quantum Dot Structures in a Hexagonal Nanowire for Quantum Photonics. 2014, 26, 2710-2717.

12.   Arbiol, J.; Magen, C.; Becker, P.; Jacopin, G.; Chernikov, A.; Schafer, S.; Furtmayr, F.; Tchernycheva, M.; Rigutti, L.; Teubert, J.; Chatterjee, S.; Morante, J. R.; Eickhoff, M. Self-assembled GaN quantum wires on GaN/AlN nanowire templates. *Nanoscale* 2012, 4, 7517-7524.

13.   Müßener, J.; Greif, L. A. T.; Kalinowski, S.; Callsen, G.; Hille, P.; Schörmann, J.; Wagner, M. R.; Schliwa, A.; Martí-Sánchez, S.; Arbiol, J.; Hoffmann, A.; Eickhoff, M. Optical emission of GaN/AlN quantum-wires – the role of charge transfer from a nanowire template. *Nanoscale* 2018, 10, 5591-5598.

14.   Heiss, M.; Fontana, Y.; Gustafsson, A.; Wüst, G.; Magen, C.; O'Regan, D. D.; Luo, J. W.; Ketterer, B.; Conesa-Boj, S.; Kuhlmann, A. V.; Houel, J.; Russo-Averchi, E.; Morante, J. R.; Cantoni, M.; Marzari, N.; Arbiol, J.; Zunger, A.; Warburton, R. J.; Fontcuberta i Morral, A. Self-assembled quantum dots in a nanowire system for quantum photonics. *Nat Mater* 2013, 12, 439-444.

15.   Mata, M. d. l.; Zhou, X.; Furtmayr, F.; Teubert, J.; Gradecak, S.; Eickhoff, M.; Fontcuberta i Morral, A.; Arbiol, J. A review of MBE grown 0D, 1D and 2D quantum structures in a nanowire. *Journal of Materials Chemistry C* 2013, 1, 4300-4312.

16.   Montinaro, M.; Wüst, G.; Munsch, M.; Fontana, Y.; Russo-Averchi, E.; Heiss, M.; Fontcuberta i Morral, A.; Warburton, R. J.; Poggio, M. Quantum Dot Opto-Mechanics in a Fully Self-Assembled Nanowire. *Nano Letters* 2014, 14, 4454-4460.

17.   Sun, B.-Q.; Zha, G.-W.; Ni, H.-Q.; Yang, S.; Shang, X.-J.; Niu, Z.-C.; Yu, Y. Self-assembled semiconductor quantum dots decorating the facets of GaAs nanowire for single-photon emission. *National Science Review* 2017, 4, 196-209.

18.   Damilano, B.; Vézian, S.; Brault, J.; Alloing, B.; Massies, J. Selective Area Sublimation: A Simple Top-down Route for GaN-Based Nanowire Fabrication. *Nano Letters* 2016, 16, 1863-1868.

19.   Han, W.; Fan, S.; Li, Q.; Hu, Y. Synthesis of Gallium Nitride Nanorods Through a Carbon Nanotube-Confined Reaction. *Science* 1997, 277, 1287.

20.   Loitsch, B.; Winnerl, J.; Grimaldi, G.; Wierzbowski, J.; Rudolph, D.; Morkötter, S.; Döblinger, M.; Abstreiter, G.; Koblmüller, G.; Finley, J. J. Crystal Phase Quantum Dots in the Ultrathin Core of GaAs–AlGaAs Core–Shell Nanowires. *Nano Letters* 2015, 15, 7544-7551.

21.   Vainorius, N.; Lehmann, S.; Gustafsson, A.; Samuelson, L.; Dick, K. A.; Pistol, M.-E. Wurtzite GaAs Quantum Wires: One-Dimensional Subband Formation. *Nano Letters* 2016, 16, 2774-2780.

22.   Haffouz, S.; Zeuner, K. D.; Dalacu, D.; Poole, P. J.; Lapointe, J.; Poitras, D.; Mnaymneh, K.; Wu, X.; Couillard, M.; Korkusinski, M.; Schöll, E.; Jöns, K. D.; Zwiller, V.; Williams, R. L. Bright Single InAsP Quantum Dots at Telecom Wavelengths in Position-Controlled InP Nanowires: The Role of the Photonic Waveguide. *Nano Letters* 2018, 18, 3047-3052.

23.   Fons, R.; Osterkryger, A. D.; Stepanov, P.; Gautier, E.; Bleuse, J.; Gérard, J.-M.; Gregersen, N.; Claudon, J. All-Optical Mapping of the Position of Quantum Dots Embedded in a Nanowire Antenna. *Nano Letters* 2018, 18, 6434-6440.

24.   Zhang, Y.; Davis, G.; Fonseka, H. A.; Velichko, A.; Gustafsson, A.; Godde, T.; Aagesen, M.; Saxena, D.; Parkinson, P.; Gott, J. A.; Yu, X.; Huo, S.; Sanchez, A. M.; Mowbray, D.; Liu, H. Highly Strained III–V–V Coaxial Nanowire Quantum Wells with Strong Carrier Confinement. *ACS Nano* 2019.

25.   Loitsch, B.; Jeon, N.; Döblinger, M.; Winnerl, J.; Parzinger, E.; Matich, S.; Wurstbauer, U.; Riedl, H.; Abstreiter, G.; Finley, J. J.; Lauhon, L. J.; Koblmüller, G. Suppression of alloy fluctuations in GaAs-AlGaAs core-shell nanowires. *Applied Physics Letters* 2016, 109, 093105.

26.   Zhang, Y.; Sanchez, A. M.; Wu, J.; Aagesen, M.; Holm, J. V.; Beanland, R.; Ward, T.; Liu, H. Polarity-Driven Quasi-3-Fold Composition Symmetry of Self-Catalyzed III–V–V Ternary Core–Shell Nanowires. *Nano Letters* 2015, 15, 3128-3133.

27.   Zheng, C.; Wong-Leung, J.; Gao, Q.; Tan, H. H.; Jagadish, C.; Etheridge, J. Polarity-Driven 3-Fold Symmetry of GaAs/AlGaAs Core Multishell Nanowires. *Nano Letters* 2013, 13, 3742-3748.

28.   Francaviglia, L.; Tütüncüoglu, G.; Martí-Sánchez, S.; Di Russo, E.; Escobar Steinvall, S.; Segura Ruiz, J.; Potts, H.; Friedl, M.; Rigutti, L.; Arbiol, J.; Fontcuberta i Morral, A. Segregation scheme of indium in AlGaInAs nanowire shells. *Physical Review Materials* 2019, 3, 023001.

29.   Jeon, N.; Loitsch, B.; Morkoetter, S.; Abstreiter, G.; Finley, J.; Krenner, H. J.; Koblmueller, G.; Lauhon, L. J. Alloy Fluctuations Act as Quantum Dot-like Emitters in GaAs-AlGaAs Core–Shell Nanowires. *ACS Nano* 2015, 9, 8335-8343.

30.   Finley, J. J.; Ashmore, A. D.; Lemaître, A.; Mowbray, D. J.; Skolnick, M. S.; Itskevich, I. E.; Maksym, P. A.; Hopkinson, M.; Krauss, T. F. Charged and neutral exciton complexes in individual self-assembled In(Ga)As quantum dots. *Physical Review B* 2001, 63, 073307.

31.   Jones, S. H.; Seidel, L. K.; Lau, K. M.; Harold, M. Patterned substrate epitaxy surface shapes. *Journal of Crystal Growth* 1991, 108, 73-88.

32.   Nishinaga, T.; Shen, X. Q.; Kishimoto, D. Surface diffusion length of cation incorporation studied by microprobe-RHEED/SEM MBE. *Journal of Crystal Growth* 1996, 163, 60-66.

33.   Verheijen, M. A.; Algra, R. E.; Borgström, M. T.; Immink, G.; Sourty, E.; van Enckevort, W. J. P.; Vlieg, E.; Bakkers, E. P. A. M. Three-Dimensional Morphology of GaP−GaAs Nanowires Revealed by Transmission Electron Microscopy Tomography. *Nano Letters* 2007, 7, 3051-3055.

34.   Caroff, P.; Dick, K. A.; Johansson, J.; Messing, M. E.; Deppert, K.; Samuelson, L. Controlled polytypic and twin-plane superlattices in III-V nanowires. *Nat. Nanotechnol.* 2009, 4, 50.

35.   Birner, S.; Zibold, T.; Andlauer, T.; Kubis, T.; Sabathil, M.; Trellakis, A.; Vogl, P. nextnano: General Purpose 3-D Simulations. *IEEE Transactions on Electron Devices* 2007, 54, 2137-2142.